Angewandte Chemie, Volume 137, Issue 21, May 2025. Article number e202424095
DOI: 10.1002/ange.202424095

Engineering Aqueous Electrolytes with Vicinal S-based Organic Additives for Highly Reversible Zinc-Ion Batteries

Teng Li,[a,c] Ahmad Naveed,[a] Jiongzhi Zheng,[d],[e] Bixian Chen,[a] Mingfeng Jiang,[a] Biyuan Liu,[e] Yu Zhou,[a] Xiaowei Li,[a] Mingru Su,[a] Ruiqiang Guo,[f] Joy Sumner,*[c] Cheng Chao Li,*[b] and Yunjian Liu*[a].

[a] T. Li, Dr. A Naveed, B. Chen, M. Jiang, Dr. Y. Zhou, Dr. X. Li, Dr. M. Su, Prof. Y. Liu
School of Materials Science and Engineering
Jiangsu University
Zhenjiang 212013, China
Email: lyjian122331@163.com (Y.L.)
[b] Prof. C. C. Li
School of Chemical Engineering and Light Industry
Guangdong University of Technology
Guangzhou 510006, China
Email: licc@gdut.edu.cn (C.C.L.)
[c] T. Li, Prof. J. Sumner
School of Water, Energy and Environment
Cranfield University
Bedfordshire MK43 0AL, UK
Email: j.sumner@cranfield.ac.uk (J.S.)
[d] Dr. J. Zheng
Thayer School of Engineering
Dartmouth College
Hanover, New Hampshire 03755, USA
[e] Dr. J. Zheng, Dr. B. Liu
Department of Mechanical and Aerospace Engineering
The Hong Kong University of Science and Technology
Kowloon 999077, Hong Kong
[f] Prof. R. Guo
Thermal Science Research Center
Shandong Institute of Advanced Technology
Jinan 250103, China

Abstract:

The commercial deployment of aqueous zinc ion batteries (AZIBs) is hampered by dendrites, the hydrogen evolution reaction (HER) and corrosion reactions. To tackle these challenges, we have introduced 3,3'-dithiobis-1-propanesulfonic acid disodium salt (SPS), a symmetrical sulfur-based organic salt, as an electrolyte additive for AZIBs. Unlike conventional electrolyte additives that favour (002) deposition, SPS enables dense (100) growth through a unique symmetrically aligned concentration-controlled adsorption network, affording structural uniformity and compactness to the Zn deposit layer. The dual-action symmetrical SPS additive adsorbs onto the Zn surface via vicinal sulfur atoms, blocking electrolyte access to the Zn anode, enhancing the transportation kinetics of Zn^{2+} and simultaneously

Published by Wiley. This is the Author Accepted Manuscript issued with: Creative Commons Attribution License (CC:BY 4.0).
The final published version (version of record) is available online at DOI:10.1002/ange.202424095. Please refer to any applicable publisher terms of use.

promoting desolvation by displacing water molecules from the solvation shell. This synergistic effect improves the stability of Zn anode by mitigating HER and corrosion, resulting in over 1100 hours of cycling at 5 mA cm^{-2}, 5 mAh cm^{-2}, stable operation at even 15 mA cm^{-2}, 15 mAh cm^{-2} and achieving impressive Coulombic efficiency (CE) of 99.41%. As validation, the Zn/$NaV_3O_8 \cdot 1.35H_2O$ cell with SPS-additive afforded high cycling stabilization and excellent capacity retention of 95.5%. This study offers valuable insights for advancing AZIBs and other metal-based batteries.

1. Introduction

Recently, the energy crisis and greenhouse gas effect have spurred the development of innovative green energy options.[1] However, the intermittent power supply problem linked to most green energy sources will severely disturb the power grid.[2] As a conventional energy storage device, battery systems are regarded as among the candidates for regulating these power grid fluctuations.[3]

In rechargeable battery technology, lithium-ion batteries (LIBs) possess the characteristic of being a mature energy storage system and are regarded as an excellent candidate for grid energy storage, thanks to the intrinsic merits of high energy density and high-level industrialization.[4] However, there exist certain critical obstacles such as high cost, low safety and environmental hazards. As an alternate, AZIBs have emerged as strong contenders for grid energy storage possessing the advantages of high theoretical capacity (820 mAh g^{-1}), high redox potential (-0.763 V vs. SHE) and abundant natural reserves of Zn anode.[5] Moreover, AZIBs benefit from the usage of aqueous electrolytes, resulting in cheap costs, excellent safety, and environmental friendliness. Therefore, AZIBs have broad application prospects in grid energy storage.[6] However, AZIBs still have problems such as short cycle life and poor reversibility of Zn anode, governed by water-borne side reactions including dendrites, HER, corrosion and shape change.

At present, the dendrite inhibition of the zinc metal anode is mainly achieved by modification of zinc anode[7], concentrated electrolytes[8] and electrolyte additives[9]. However, the preparation of 3D zinc anode designs is intricate and often incurs a significant expense. Concentrated electrolytes can effectively stabilize the Zn anode but their increased costs and higher viscosity limit the practical utilization. In addition, the high salt/water ratio can lead to a low ionic conductivity, which harms the rate performance and energy density of AZIBs.[8, 10]

Typical zinc anode optimization such as coating or 3D anode design can effectively inhibit dendrite growth, the HER and Zn corrosion.[11] However, at high zinc deposition capacities when matched with a

high mass loading cathode, the coating is susceptible to failure due to the reciprocating stress during the plating/stripping resulting in short cycle life.[12] In addition, the transport rate of Zn^{2+} in organic coatings is usually smaller than that in aqueous electrolytes, which will increase the polarization voltage.[11a] Among all the Zn anode stabilization strategies discussed above, the adoption of electrolyte additives appears highly efficient and simple route.

Electrolyte engineering through additives can efficiently and extensively adjust the solvation structure of zinc ions in the aqueous electrolyte, not only at the anode interface. Besides, the electrolyte additive can continuously guide the uniform deposition of zinc onto the zinc anode to form a smooth and dendrite-free surface, even at a high electroplating depth. Therefore, the application of the electrolyte additives has a bright prospect in high-performance AZIBs.

The protection strategy of electrolyte additives through interfacial adsorption for suppressing dendrites and side reactions has been widely studied. The electrolyte additives such as D-phenylalanine (DPA)[5a], tetraphenylporphyrin tetrasulfonic acid (TPPS)[13], 1-butyl-3-methylimidazolium cation ($BMIm^+$)[14], disodium maleate (DMA)[15], hexamethylphosphoramide (HMPA),[16] and amikacin sulfate (AS)[17] preferentially adsorb on the surface of the zinc anode by competing with $[Zn(H_2O)_6]^{2+}$ to form an ionic layer. The adsorbed layer is proposed to regulate the zinc flux at Zn-electrolyte interface, therefore guiding uniform deposition. Besides, the adsorption layer could isolate the contact between the electrode and water molecules inhibiting the HER and electrode corrosion. However, the physisorption layer is prone to desorption during the continuous deposition of zinc, especially under high current densities.

Recently, the improvement strategies of sulfonic acid-based additives have attracted a great deal of attention. For instance, sodium dodecyl sulfate (SDS) containing sulfonic acid offered good electrostatic adsorption on the zinc surface through sulfonic acid groups.[18] Zheng et al. also demonstrated that the sodium methylenedinaphthalene disulphonate (SMD) additive has an adsorption preference over $[Zn(H_2O)_6]^{2+}$ by investigating the adsorption mechanism.[19] In addition, this study proposed that the sulfonic acid group can form coordination bonds with Zn^{2+} to replace H_2O in $[Zn(H_2O)_6]^{2+}$.[19] However, most sulfonates, such as SDS, sodium dodecyl benzene sulfonate (SDBS), sulfolane (SL) and dimethyl sulfoxide (DMSO), only have a sulfonic acid group at the end of the organic linker or even do not have a sulfonic acid group at any end of the linker.[18, 20] This will lead to a single absorption site for the sulfonic acid group, which can separate the $[Zn(H_2O)_6]^{2+}$ and anode to inhibit the HER and corrosion. However, the aliphatic chains in these absorption layers will increase the Zn^{2+} transportation resistance leading to increased polarization.[20]

In this paper, SPS (3,3'-dithiobis-1-propanesulfonic acid disodium salt) with a symmetrical $-SO_3^-$

structure was designed to act as an electrolyte additive for AZIBs. To improve the adsorption stability, a 0.2 M concentration was selected to alleviate the physical desorption on Zn anode for the SPS additive. Impressively, the symmetrical cells can stably cycle for 1120 hours with a low separator thickness of 110 μm at 5 mA cm^{-2}, 5 mAh cm^{-2}. According to the experiments and calculations, this strategy can strongly guide the uniform deposition of Zn^{2+} and alleviate the desorption of the absorbed layer constructed by the SPS additive as shown in Fig. 1. Moreover, SPS can reconstruct the hydrogen bond network structure by replacing the water sheath in $[Zn(H_2O)_6]^{2+}$ in the electrolyte, which can provide a desolvation process to inhibit the HER. Besides, the SPS adsorbed on the surface of the zinc anode can effectively isolate the contact between the free water and zinc foil to act as a protecting layer, which can further inhibit the HER and corrosion. Different to the other typical additives with sulfonic acid groups, which will hinder the transport of Zn^{2+}, the addition of SPS can reduce the Zn^{2+} transport resistance through the grasping effect of symmetrical $-SO_3^-$ structure. Impressively, a dense (100) deposition was found in $ZnSO_4$-SPS system different from the typical (002) deposition which could not only avoid short-circuit but also decrease the contact area of zinc with electrolyte to suppress side reactions.

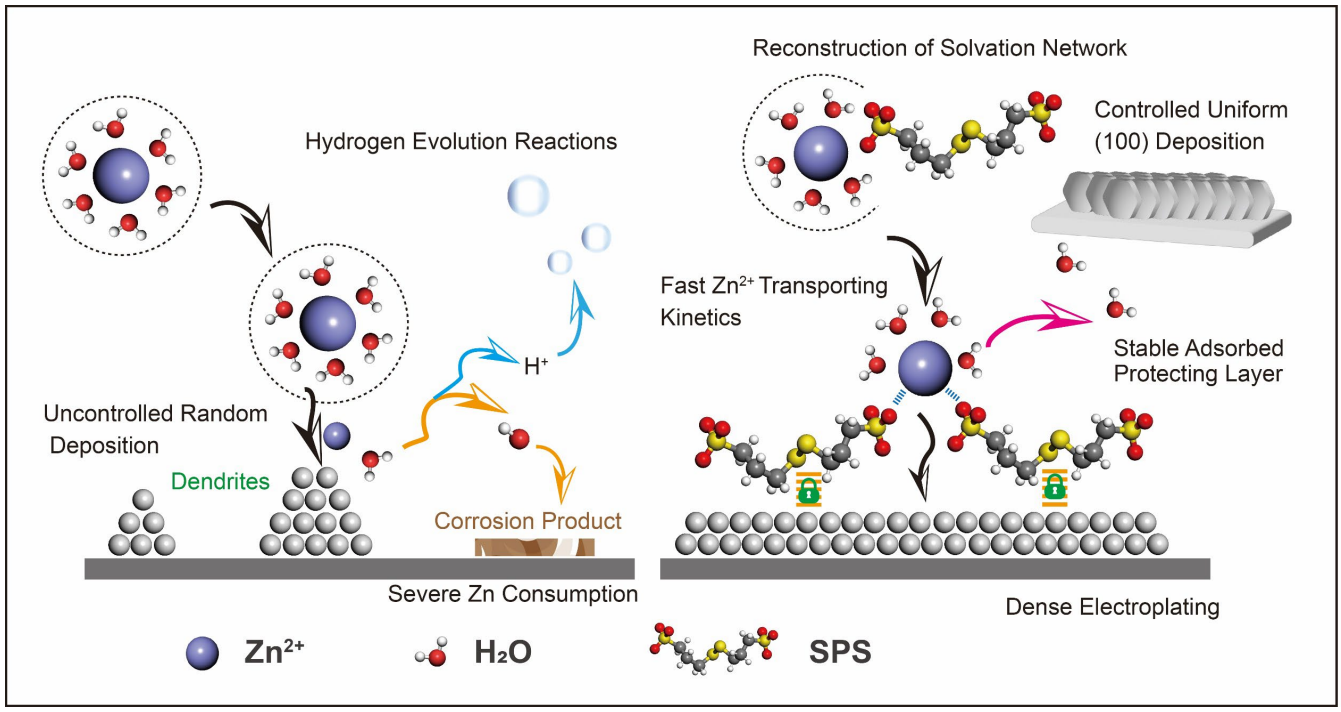


Figure 1. Schematic illustration of the suppression of dendrites and side reactions achieved by the dynamic adsorption of SPS.

2. Results and discussion

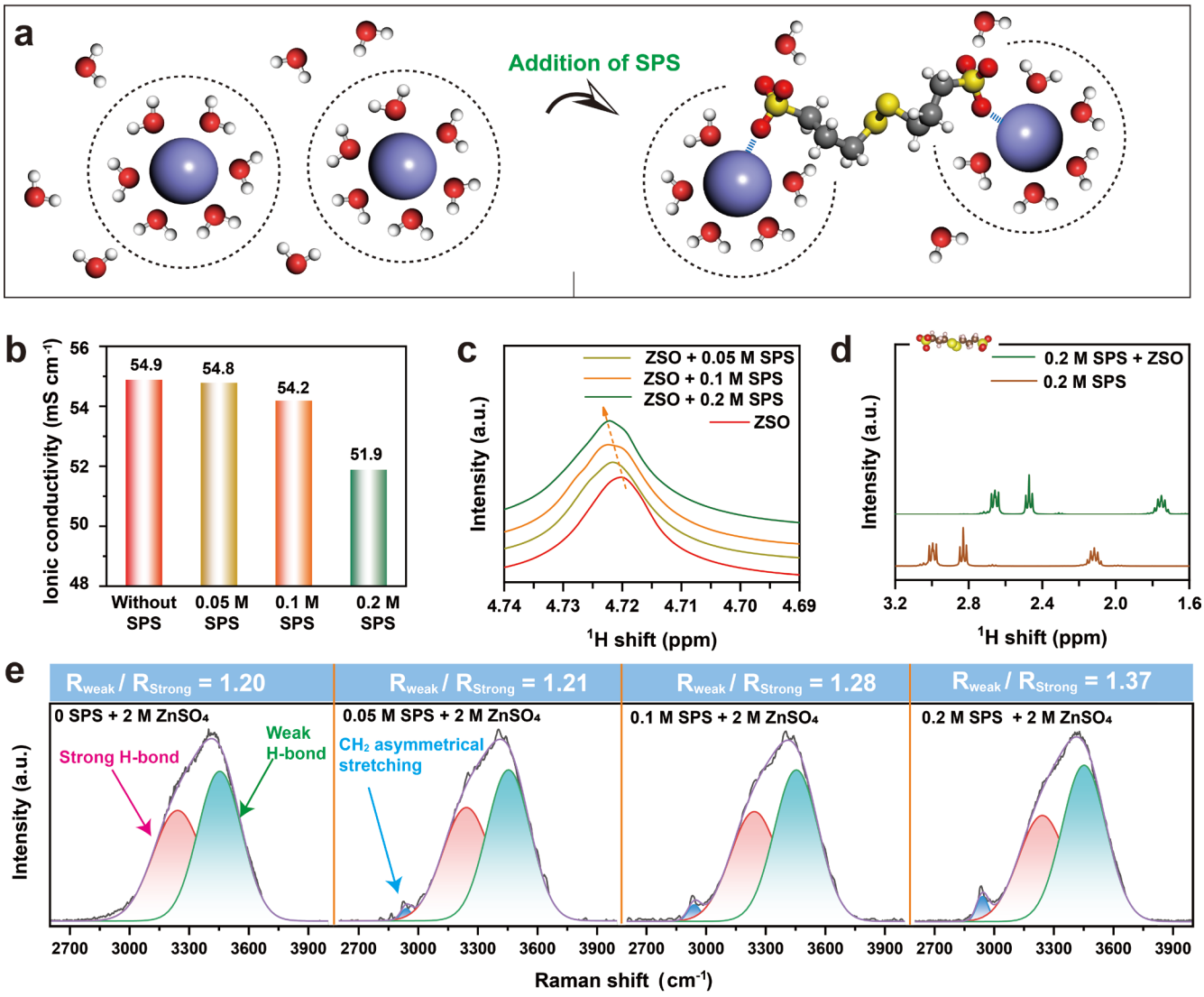


Figure 2. The reconstruction effect of SPS on solvation network. (a) Schematic diagram. (b) The ionic conductivities measured for $ZnSO_4$ and $ZnSO_4$-SPS electrolytes. (c) ^1H nuclear magnetic resonance spectroscopy (NMR) of $ZnSO_4$ without and with SPS. (d) ^1H NMR results of $ZnSO_4$ without and with 0.2 M SPS dissolved in D_2O. (e) Fitting results of Raman spectrum without and with SPS in $ZnSO_4$ electrolyte, respectively (The blue peaks: CH_2 asymmetrical stretching from SPS[21]).

Fig. 2a is the schematic diagram of the SPS reconstructing the solvation network. $-SO_3^-$ located at both ends of SPS can replace the solvated water around Zn^{2+} to destroy the water sheath and reconstruct the solvation network. As shown in Fig. 2b, the conductivity decreased from 54.9 mS cm^{-1} to 51.9 mS cm^{-1} as the SPS concentration increased from 0 to 0.2 M in 2 M $ZnSO_4$. The decrease in ionic conductivity indicates that the binding of Zn^{2+} in the electrolyte increases with the increase of SPS, and the transport

process is turned to control. It is worth noting that the transfer rate above 50 mS cm^{-1} is still high compared to the solid and organic systems to ensure fast Zn^{2+} transportation kinetics in electrolytes. To observe the effect of SPS additive on the solvation structure of Zn^{2+}, ^{1}H NMR testing was introduced as shown in Fig. 2c. The ^{1}H NMR results show that the peak shifts towards a low magnetic field with the increase of SPS concentration. The ^{1}H NMR peak of the $ZnSO_4$ solution emerged at 4.719 ppm and then shifted to 4.725 ppm after 0.2 M SPS addition which suggested that $ZnSO_4$ with SPS electrolyte could provide a stronger de-shielding effect. The anion forms strong hydrogen bonds with the water molecules among free water molecules, which weakens the shielding effect caused by the electron cloud around the hydrogen atoms.[22] SPS could contribute to the reconstruction of H-bond networks. Besides, the ^{1}H NMR signal of $ZnSO_4$-SPS shifts towards a higher field compared to SPS as shown in Fig. 2d, which is due to the interaction between SPS and Zn^{2+} driven by the electron-withdrawing effect.[13, 23] The Raman spectrum of O-H bonds is in the range of 2800-3800 cm^{-1} which is divided into strong (3242 cm^{-1}) and weak (3454 cm^{-1}) hydrogen bonds in Fig. 2e.[24] The ratio of weak H-bonds to strong H-bonds in $ZnSO_4$-0.2 M SPS is 1.37, which was higher than that of $ZnSO_4$ (1.20), indicating that the introduction of SPS could destroy the solvation network structure in the $ZnSO_4$ electrolyte and reduce the reactivity of free water.[25] The reconstruction of the H-bond network will suppress the HER as a competing reaction to Zn deposition.

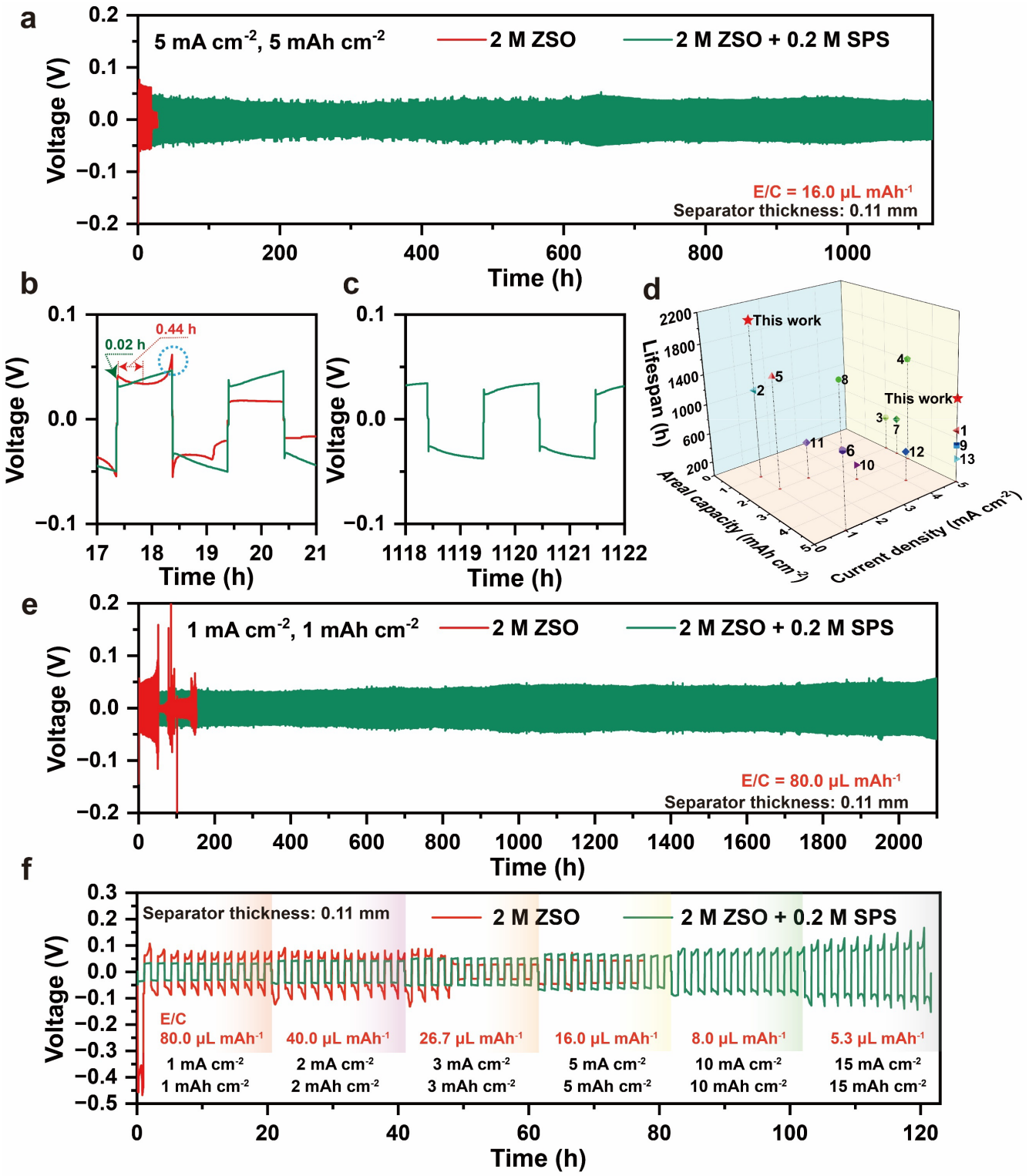


Figure 3. Cycling stability of Zn/Zn symmetric cells with the addition of SPS with GF/A separator. (a) Galvanostatic cycling performance at 5 mA cm^{-2}, 5 mAh cm^{-2}. (b, c) Corresponding Voltage-time curves. (d) The electrochemical performance compared to other publications. (e) Cycling stability at 1 mA cm^{-2}, 1 mAh cm^{-2}. (f) Rate capability at different current densities (from 1 mA cm^{-2}, 1 mAh cm^{-2} to 15 mA cm^{-2}, 15 mAh cm^{-2}).

The role of SPS additive towards inhibition of Zn dendrites and side reactions was first investigated

by subjecting symmetrical Zn/Zn cells to cycling at different applied current densities. The selection of separator is GF/A, and its actual thickness after pressure application is approximately 0.11 mm (Fig. S2) and a low electrolyte dosage (80 μL) can achieve high volumetric and gravimetric energy densities, respectively. However, batteries with GF/A are more prone to short circuits due to lower separator thickness.

As shown in Fig. 3a, the symmetrical battery with 0.2 M SPS additive can stably cycle for 1120 h at 5 mA cm^{-2}, 5 mAh cm^{-2} indicating a strong inhibition effect of Zn dendrites in the system. Compared to other additive concentrations (0.05, 0.1 and 0.4 M) of SPS, 0.2 M has the best performance for over 1100 h among the researched concentrations as shown in Fig. S3. As a comparison, the Zn/Zn cell in $ZnSO_4$ electrolyte only cycled for 18 h before experiencing an internal short-circuit. In addition, the voltage curves of Zn plating/striping obtained in $ZnSO_4$ electrolyte are obviously unsymmetrical due to the side reactions.[26] Fig. 3b shows that the cells without SPS have a sharp polarization voltage increase in the blue circle, indicating a significant zinc consumption and the generation of inert products due to side reactions which lead to a more difficult stripping and plating. Additionally, an obvious prolonged nucleation time (0.44 h) was observed in $ZnSO_4$ system in Fig. 3b. However, with the addition of SPS to the system, the symmetrical cell has a short nucleation time (0.02 h) indicating a quick construction of the initial deposition layer corresponding to the strong guided plating due to the regulation effect of SPS. Besides, the subsequent zinc deposition process is stable demonstrating that no obvious side reactions occur. Even cycled for over 1100 h at 5 mA cm^{-2}, 5 mAh cm^{-2}, the shape of plating/stripping curves (Fig. 3c) still remained symmetrical and no obvious fluctuation or large polarization was observed suggesting a strong cycling stability of Zn anode in SPS added cells. Moreover, there was a decrease in the overpotential for $ZnSO_4$-SPS system in Fig. 3c compared to Fig. 3b which could be attributed to the different degrees of roughness of the Zn foil at different cycling times.

Compared with other works focusing on electrolyte additives, the cycling life and stability of this work with SPS additives are still impressive as shown in Fig. 3d and Table. S1. In addition, as shown in Fig. 3e, the cycling life of the system with SPS can reach 2100 h at 1 mA cm^{-2}, 1 mAh cm^{-2} which is much better than the system without SPS (50 h) indicating a strong inhibition of dendrites at low current density as well. In addition, high DOD (45.4%) work condition was also employed to evaluate the zinc consumption during the cycling in Fig. S4. The result shows that the cell could stably cycle around 80 h in $ZnSO_4$-SPS electrolyte at a high current density of 15 mA cm^{-2} (with a low E/C ratio of 5.3 μL mAh^{-1}). As a comparison, the cell with $ZnSO_4$ could only cycle around 1 h before got short-circuit. The prolonged cycling life demonstrates that the SPS additive could significantly inhibit the dendrites and suppress the side reactions to alleviate zinc consumption. The current tolerance of Zn anode was

examined by rate capability test of the symmetrical cells with and without SPS additive in aqueous electrolyte, the applied current density was systematically increased from 1 mA cm^{-2}, 1 mAh cm^{-2} to 15 mA cm^{-2}, 15 mAh cm^{-2} as displayed in Fig. 3f. The rate performance result shows the cell without SPS additive was short-circuit due to the growth of dendrites at 3 mA cm^{-2} (Fig. S5), and the polarization voltage is obviously turn to asymmetry over 2 mA cm^{-2}. In contrast, the SPS additive system can operate stably even at a high current density of 15 mA cm^{-2} and maintain a good symmetrical shape (Fig. S6). The exchange current density was also calculated in Fig. S7. The cell in $ZnSO_4$-SPS system exhibits a higher exchange current density (8.18 mA cm^{-2}) compared to the $ZnSO_4$ (4.09 mA cm^{-2}), demonstrating a fast electroplating/stripping reaction dynamic for the lower energy barrier.

The apparent differences indicate that SPS additives can provide a strong effect on the homogeneous distribution of the electric field on the surface of zinc foil and guide the uniform deposition of zinc as well as avoiding the occurrence of dendrites and side reactions. SPS additive significantly enhances the cycling life of Zn anodes across various current densities by promoting uniform Zn deposition and parasitic side reactions. To examine the morphological evolution of Zn anode cycled with and without SPS additive, scanning electron microscopy (SEM) and atomic force microscopy (AFM) analysis were conducted (Supplementary Note. 2-3).

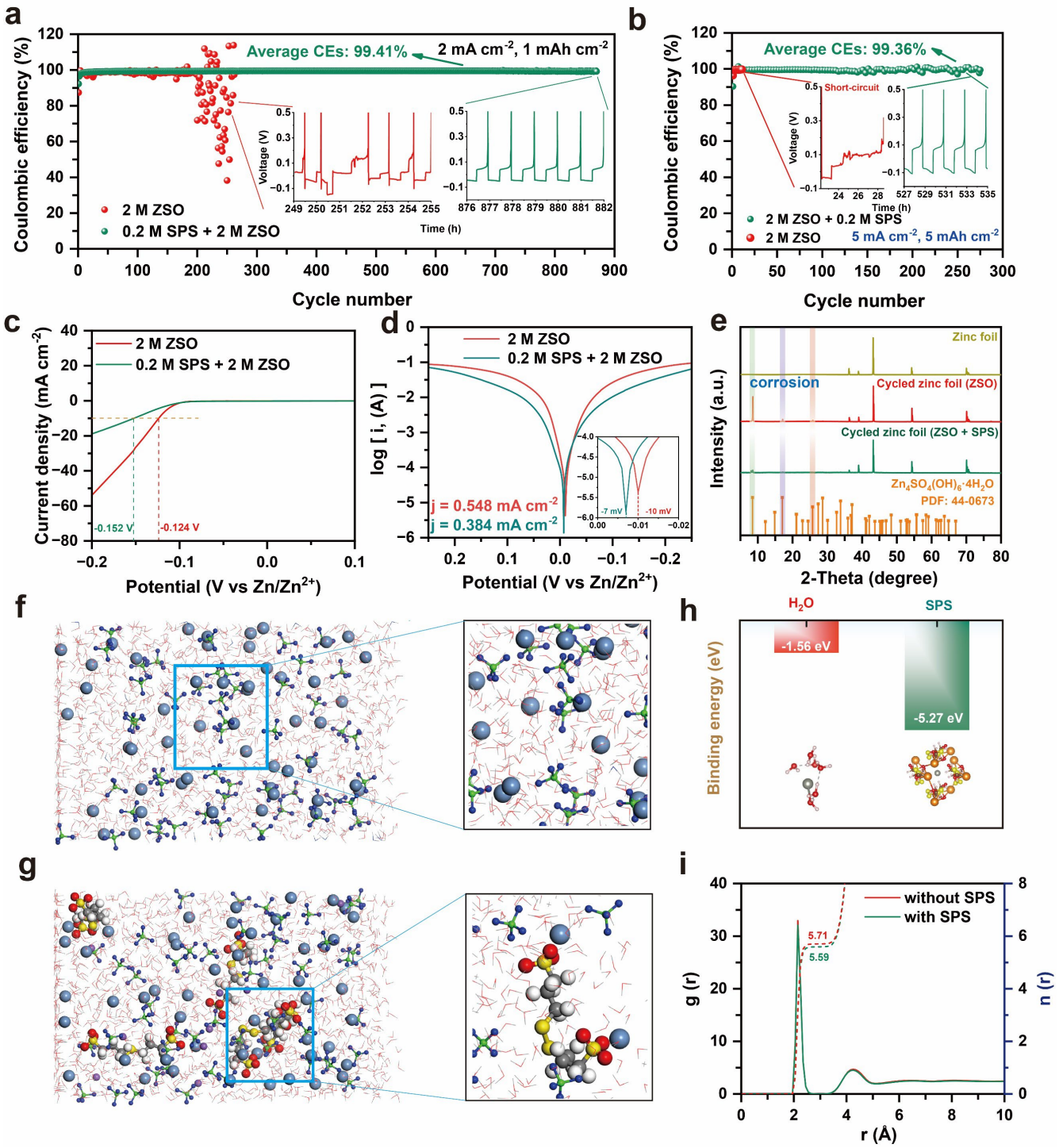


Figure 4. Reversibility optimization of AZIBs with the addition of SPS. (a, b) The cycling performance of Zn/Cu cells in $ZnSO_4$ and $ZnSO_4$-SPS electrolyte with a cut-off voltage of 0.5 V at 2 mA cm^{-2}, 1 mAh cm^{-2} and 5 mA cm^{-2}, 5 mAh cm^{-2}, respectively. (c) Linear sweep voltammetry (LSV) test with and without SPS at a scan rate of 5 mV/s. (d) Tafel test at a scan rate of 5 mV/s. (e) XRD result of zinc foil after 40 cycles at 1 mA cm^{-2}, 1 mAh cm^{-2}. (f, g) Molecular Dynamics Simulation (MD) of $ZnSO_4$ and $ZnSO_4$-SPS electrolyte, respectively. (h) Binding energy of Zn^{2+} with H_2O and SPS by density functional theory (DFT) calculations. (i) Radial distribution function (RDF) plots for the above two systems according to MD results.

To explore the effect of SPS additives on the reversibility of zinc anode, Zn/Cu asymmetric cells were cycled at different current densities (1, 2 and 5 mA cm^{-2}). From the CE results in Fig. S11 and Fig. 4a, the $ZnSO_4$ system can only work stably for 418 cycles and 165 cycles at 1 and 2 mA cm^{-2} current densities, respectively, and then the system will become unstable or even short-circuited. In contrast, the $ZnSO_4$-SPS system can stably cycle for more than 1200 and 850 times along with delivering average CEs of 99.08% and 99.41%, respectively, reflecting long cycling life and high reversibility.

Compared with symmetrical batteries, Zn/Cu asymmetric batteries can better reflect the actual life of Zn anode because of the limited zinc reserve in the system.[27] In this regard, the Zn/Cu asymmetric test at 5 mA cm^{-2}, 5 mAh cm^{-2} was designed to aggravate the conditions for the side reactions, and the results suggested the Zn/Cu asymmetric battery with $ZnSO_4$ electrolyte could stably work for 11 cycles (Fig. 4b). From the enlarged graph, an obvious delay occurs at 0.1 V which proves that the cell suffered a short circuit. On the other hand, the Zn/Cu cell with $ZnSO_4$-SPS has a long cycling life of more than 250 cycles with high average CEs of 99.36%. The cycling curve over 250 cycles is still stable and regular which illustrates a strong inhibition of dendrites growth and zinc consumption.

The reversibility of the Zn anode is impaired by the HER and the corrosion reaction. LSV was used to explore the HER on the anode as shown in Fig. 4c. To reach the HER current of 10 mA cm^{-2}, the addition of SPS can extend the hydrogen evolution potential to -0.152 V while the potential of $ZnSO_4$ system is -0.124 V, which significantly widens the electrochemical stability window of AZIBs. The results show that the HER rate of the $ZnSO_4$-SPS system was significantly lower than that of $ZnSO_4$, indicating that the SPS had a significant suppression effect on the HER which competes with zinc deposition. The Tafel test of zinc foil in $ZnSO_4$ and $ZnSO_4$-SPS was carried out to explore the effect of SPS on corrosion reactions. Corresponding to Fig. 4d, the corrosion current density of $ZnSO_4$ is 0.548 mA cm^{-2}, while the corrosion current of $ZnSO_4$-SPS is 0.384 mA cm^{-2}, indicating that the addition of SPS reduces the corrosion reaction rate. Moreover, the corrosion potential of $ZnSO_4$-SPS is -7 mV, which is obviously lower than that of $ZnSO_4$ (-10 mV), indicating that SPS can attenuate the tendency of corrosion reaction. Furthermore, the suppression of the corrosion reactions during the cycling was researched in Fig. 4e. The XRD results of the zinc anode in $ZnSO_4$ showed a strong corrosion peak after 40 cycles, corresponding to $Zn_4SO_4(OH)_6{\cdot}4H_2O$ (JCPDS: 44-0673), indicating that severe corrosion reaction occurred during cycling without protection. However, only slight corrosion peaks were observed in the zinc foil protected by SPS, indicating that SPS had a significant inhibitory effect on corrosion reactions. The grazing-incidence wide-angle X-ray scattering (GIWAXS) results further proved the marked suppression effect on corrosion provided by SPS in Fig. S13.

An electrochemical impedance spectroscopy (EIS) test was employed to examine the transport

kinetics of Zn^{2+} at the electrolyte-anode interface. As shown in Fig. S14(a, b), the charge transfer impedance of SPS is 263.9 Ω at 30 ℃, which is much lower than that of SPS (1836 Ω), indicating that SPS can significantly reduce the transport kinetics of zinc ions due to de-solvation. As shown in Fig. S14c, the activation energy of $ZnSO_4$-SPS electrolyte was 38.4 kJ/mol, which was lower than that of the $ZnSO_4$ system (49.5 kJ/mol), indicating that SPS could reduce the interfacial de-solvation energy barrier and accelerate the de-solvation process of zinc.

To further explore the de-solvation effect of SPS, MD was set for systems without and with 0.2 M SPS in 2 M $ZnSO_4$ electrolyte, respectively, as shown in Fig. 4(f, g). The results showed that SPS could provide a de-solvation effect to replace the solvated water around Zn^{2+} and reconstruct the solvation networks. The DFT calculation results (Fig. 4h) suggest SPS have a strong binding effect with Zn^{2+} (-5.27 eV) compared to H_2O molecules (-1.56 eV), indicating SPS can re-construct the sheathes of $[Zn(H_2O)_6]^{2+}$ by replacing the position of H_2O. The RDF results as shown in Fig. 4i suggest that the characteristic peak of Zn-O in the range of 1.95-2.55 Å in both systems. The average coordination number (ACN) between water molecules and Zn^{2+} in the SPS system was 5.59 which is lower than that in the SPS-free system (5.71), indicating that Zn^{2+} and SPS had a stronger binding effect than water and the addition of SPS could reduce the amount of solvated water in the system.

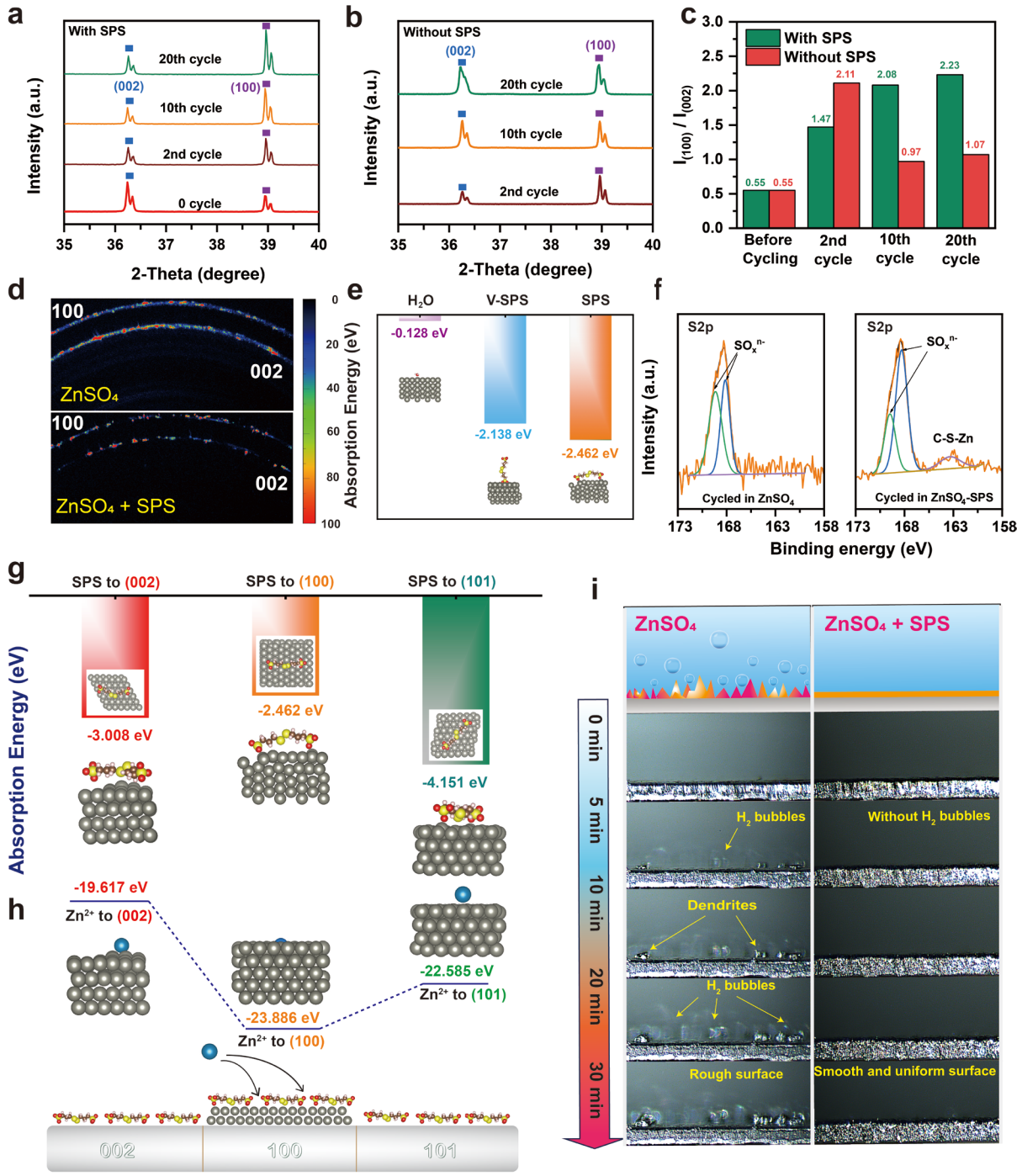


Figure 5. The mechanism of the dendrite-free anode in $ZnSO_4$-SPS electrolyte. (a, b) The XRD results of the Zn foil after 0, 2, 10 and 20 cycles with and without 0.2 M SPS, respectively. (c) The XRD peak intensity ratios of the (100) and (002) crystal planes after different cycles in $ZnSO_4$ and $ZnSO_4$-0.2 M SPS systems. (d) The GIWAXS results of the zinc foils cycled in 2 M $ZnSO_4$ and $ZnSO_4$-0.2 M SPS systems. (e) The DFT Calculation of the adsorption energy of H_2O, vertical-SPS and SPS on Zn (100) plane. (f) The XPS S 2p spectra of zinc foils after 10 cycles in $ZnSO_4$ and SPS-$ZnSO_4$, respectively. (g, h) Binding energies of SPS and Zn^{2+} on (002), (100) and (101), respectively. (i) The in-situ optical results of Zn anode cycled in $ZnSO_4$ electrolyte with and without SPS at a high current density of 15 mA cm^{-2}, respectively.

XRD patterns were employed to determine the main deposition mode in $ZnSO_4$-SPS and $ZnSO_4$ at different stages of 2, 10, and 20 cycles as shown in Fig. 5a and 5b, respectively. The XRD results show that with the addition of 0.2 M SPS, the deposition mode of zinc is mainly high-index (100). As the cycling increased, the characteristic peaks of the low-index (002) plane gradually decreased and the characteristic peaks of the high-index (100) plane gradually increased. In Fig. 5c, the peak intensity ratios ($I_{(100)}/I_{(002)}$) were performed. The results show that the $I_{(100)}/I_{(002)}$ increases from 0.55 to 2.23 as the cycle number increases from 0 to 20 demonstrating that the (100) plane is the main deposition plane in $ZnSO_4$-SPS system. Compared to (002) deposition, the (100) plane has the highest adsorption energy as well as the lowest stripping energy demonstrating that could achieve a fast electroplating\stripping dynamic.[28] For $ZnSO_4$, the regularity was not found after the same cycles illustrating a random and uncontrolled deposition. To better verify the deposition style, the GIWAXS results of zinc foil after cycling in $ZnSO_4$ and $ZnSO_4$-SPS were compared in Fig. 5d. The strength of the (100) diffraction signal is stronger than that of (002) in $ZnSO_4$-SPS system which proved the main (100) deposition. Compared with the $ZnSO_4$ system, the signal of zinc foil cycled in SPS-$ZnSO_4$ is more concentrated suggesting a highly controlled deposition with a higher consistency of orientation.[29]

To explore the adsorption-guided deposition mechanism, the adsorption energy of H_2O, vertical-SPS and SPS on the zinc anode were calculated by DFT and plotted in Fig. 5e. The results show that SPS has a strong adsorbing preference (-2.462 eV) with zinc anode compared to water (-0.128 eV) indicating that SPS will preferentially adsorb to the zinc surface to form a protective layer during the static and cycling process of the cell. To determine the adsorption style of SPS, the adsorption energies of vertical -SPS and horizontal-SPS on Zn were compared. The results show that the adsorption energy of horizontal-SPS (-2.462 eV) is higher than that of vertical-SPS (-2.138 eV) demonstrating horizontal-SPS to be the main adsorption style on Zn achieved by multiple adsorption sites during the electroplating and stripping process. This is due to the special position of the -S-S- group in the centre of the SPS, which acts as a “lock” in enhancing adsorption. Benefitting from this special adsorption mechanism, the covering area of the same concentration additive could be maximized. Besides, the Zn^{2+} could combined with SO_3^- groups which are at both ends of the SPS to form the network to guide the uniform deposition and provide strong protection for the zinc anode. To verify this enhancement, the XPS results of zinc foil cycled in $ZnSO_4$ and $ZnSO_4$-SPS are shown in Fig. 5f. In addition to the SO_x^{n-} peaks (168-170 eV)[30], a significant C-S-Zn peak (163.3 eV) in $ZnSO_4$-SPS aroused, indicating that the -S-S- group could supply a stable adsorbing function on the Zn anode.[31]

To explore the deposition mechanism, the adsorption energy of SPS for different crystal planes was calculated, as shown in Fig. 5g. The results showed that the SPS had the highest adsorption energy (-

4.151 eV) for (101) and the lowest (-2.462 eV) for (100). Compared to (100), SPS preferentially adsorbs on (101) and (002) planes, leaving the (100) plane relatively more exposed and preferred for Zn plating in the case of the addition of trace amounts of SPS as shown in Fig. S16. However, due to the lack of SPS covering on (100), there is a risk of uncontrollable deposition of zinc anode and corrosion.[32]

In the case of the addition of an appropriate amount of SPS (0.2 M), considering that the adsorption energy of SPS-Zn is much higher than that of H_2O, the $ZnSO_4$-SPS system could achieve uniform adsorption on the surface of the zinc foil anode, as shown in Fig. 5h. In addition, the adsorption energies of Zn^{2+} on (002), (100) and (101) were calculated in Fig. 5h. The adsorption energy on (100) (-23.886 eV) was significantly greater than that of (002) (-19.617 eV) and (101) (-22.585 eV). The uniform and controllable at (100) plane could be achieved. Chronoamperometry (CA) and morphologies were also discussed in Supplementary Note. 8 as proof of the mechanism. Typical uncontrolled high index (100/101) deposition such as cycled in $ZnSO_4$ electrolyte could lead to a loose and ununiform deposition which is easy to penetrate the separator. However, the (100) deposition guided by SPS is dense and uniform as proved in Fig. S19 which is regulated by the guiding network through the adsorption of SPS.

To visually verify the inhibitory effect of SPS additives on dendrite and side reactions, the zinc anode was observed at 15 mA cm^{-2} by in-situ optical microscopes, as seen in Fig. 5i. For the $ZnSO_4$ system, substantial bubbles and large-size dendrites (non-uniform distribution) were found at the anode-electrolyte interface. With the addition of SPS, the thickness of the deposited Zn layer increased uniformly, and no obvious dendrites and HER bubbles were observed.

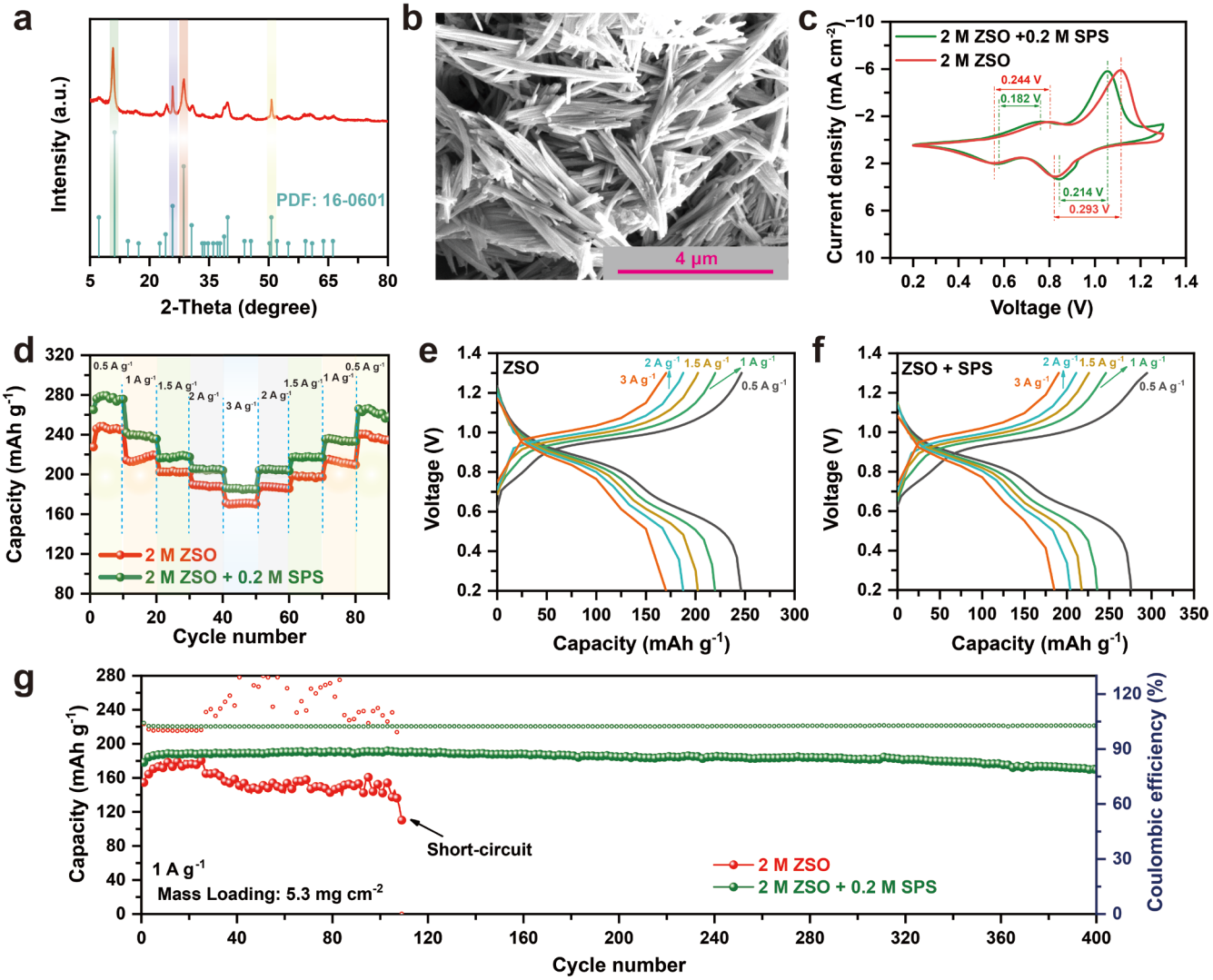


Figure 6. The galvanostatic cycling performance of the Zn/$NaV_3O_8 \cdot 1.35H_2O$ (NVO) full cells. (a) The XRD result of NVO with corresponding standard JCPDS card. (b) The nanoribbon micro-structure of the synthesized NVO. (c) Cyclic voltammetry (CV) curves of the Zn/NVO battery in $ZnSO_4$ and $ZnSO_4$-SPS electrolytes at a scan rate of 0.5 mV/s, respectively. (d) Rate performance of the Zn/NVO cell at the current density of 0.5, 1, 1.5, 2 and 3 A g^{-1}, respectively. (e, f) Corresponding galvanostatic charge/discharge (GCD) curves in $ZnSO_4$ and $ZnSO_4$-SPS systems of the rate tests, respectively. (g) Long cycling tests for Zn/NVO full batteries at 1 A g^{-1} with a mass loading of 5.3 mg cm^{-2}.

As a validation, the full cells were tested with $ZnSO_4$ and $ZnSO_4$-SPS as electrolytes, respectively. The Zn anode was coupled with NVO cathode material, and the corresponding XRD pattern of the as-prepared NVO cathode is shown in Fig. 6a. The characteristic peaks of the synthesized NVO are matched with the standard card (PDF:16-0601), indicating the crystal structure and crystallinity correspond to sodium vanadate (NVO). The synthesized NVO as shown in Fig. 6b illustrates a typical nanoribbon morphology, which is conducive to zinc transport. Fig. 6c shows the CV curves of $ZnSO_4$ and $ZnSO_4$-

SPS at a sweep speed of 0.5 mV/s. The shape remains approximately the same, indicating that the addition of SPS does not alter the redox reactions of V^{5+}/V^{4+} and V^{4+}/V^{3+} on the V-based cathode. In addition, the characteristic peak differences of V^{5+}/V^{4+} and V^{4+}/V^{3+} peaks of $ZnSO_4$-SPS during charging and discharging were 0.214 V and 0.182 V, respectively, which were smaller than those of $ZnSO_4$ system at 0.293 V and 0.244 V. The decrease in the voltage difference between charging and discharging indicates that the addition of SPS could reduce the polarization inside the full battery. The rate performance is employed to evaluate the performance at different current densities related to the fast charging/discharging ability. From Fig. 6d, the rate performance of $ZnSO_4$-SPS is higher than that of $ZnSO_4$, and the capacity is maintained well when the capacity recovers well after the cycling at high current density which reflects the stability of the full cell. At the current of 0.5, 1, 1.5, 2 and 3 A g^{-1}, the capacities of $ZnSO_4$-SPS are 276, 235, 217, 203 and 185 mAh g^{-1}, respectively, which are significantly higher than those of $ZnSO_4$ (246, 220, 202, 187 and 170 mAh g^{-1}). The voltage-capacity curves for the rate performance in $ZnSO_4$ and $ZnSO_4$-SPS systems are shown in Fig. 6(e, f), respectively. The charge-discharge curves of $ZnSO_4$-SPS system are well maintained and there is still an obvious plateau compared with $ZnSO_4$ under the high current of 3 A g^{-1}, indicating that the addition of SPS can improve the rapid charge-discharge ability of AZIBs. In addition, to better evaluate the stability of zinc batteries, a high active material loading of 5.3 mg cm^{-2} was employed for testing as shown in Fig. 6g. The result demonstrates that the CEs of NVO/Zn batteries with $ZnSO_4$ electrolyte after 25 cycles is significantly unstable, which is weakened by the severe corrosion of the zinc foil surface to generate plenty of irreversible basic zinc sulfate. After 110 cycles, a noticeable short-circuit occurred. The $ZnSO_4$-SPS battery can stably work for 400 cycles, with a capacity of 170 mAh g^{-1} and great capacity retention of 95.5%. The results demonstrate that the addition of SPS can significantly inhibit the dendrite growth and side reactions on the zinc anode, and prolong the cycling life and stability of AZIBs.

3. Conclusion

In summary, an electrolyte additive strategy is proposed in this work to adjust the interfacial deposition of zinc and the solvation structure of the electrolyte in AZIBs. Specifically, SPS is employed to achieve dendrite-free and highly reversible zinc anodes. The mechanism involves SPS induced symmetrical adsorption network on the zinc anode through -S-S- group, while the terminal $-SO_3^-$ facilitates uniform Zn^{2+} transport and electric field distribution, the dual synergistic effect affords dense and controlled zinc deposition. XRD, GIWAXS and SEM analysis confirm that zinc predominantly deposits on (100) planes in the SPS-containing system, contrasting with (002) orientation commonly promoted by other electrolyte additives. The symmetrical cell with SPS can be stably cycled for more

than 1100 hours at 5 mA cm^{-2}, 5 mAh cm^{-2} and even sustain a high current density of 15 mA cm^{-2}, 15 mAh cm^{-2} with the thin glass fibre separator (GF/A), demonstrating a strong ability to inhibit dendrites. Experimental and MD calculations demonstrate that SPS inhibits the HER in three ways: first by adsorbing onto the anode to form a dynamic protective layer that isolates water from Zn surface; second, by replacing water molecules in the Zn^{2+} solvation shell via de-solvation effect; and third, by reorganizing the hydrogen bond structure to reduce the proportion of active water in the electrolyte. The in-situ optical test gives intuitive and strong proof for the suppression of HER by these three routes. Additionally, the corrosion experiments have demonstrated that SPS exhibits a significant inhibitory effect on Zn corrosion. Finally, Zn/ NVO full cells were assembled to verify the inhibition of SPS on dendrites and HER. The results showed that the SPS-supplemented system could achieve high rate-performance, long cycle life and stability. Notably, a high-capacity retention rate of 95.5% was achieved at a high mass loading of 5.3 mg. This work can provide valuable ideas for the development of metal-based aqueous batteries.

Conflict of Interest

The authors declare no conflict of interest.

Acknowledgements

T.L., A.N. and J.Z. contributed equally to this work. The work was supported by the National Natural Science Foundation of China (22350410378 and 52274299).

Data Availability Statement

The data that support the findings of this study are available from the corresponding author upon reasonable request.

Keywords: Aqueous zinc-ion batteries • Dendrite-free • Dynamic adsorption • Vertical (100) deposition • Electrolyte additives.

Reference

[1] a) J. Zhu, Z. Tie, S. Bi, Z. Niu, *Angew. Chem. Int. Ed.* **2024**, *63*, e202403712; b) C. Wang, G. He, J. Meng, S. Wang, Y. Kong, J. Jiang, R. Hu, G. Zhou, *GCB Bioenergy* **2020**, *12*, 1066-1077; c) W. Huang, X. He, J. Wu, X. Ma, J. Han, L. Wang, Y. Wang, *Ind. Crops Prod.* **2023**, *197*, 116555.

[2] a) T. M. Gür, *Energy Environ. Sci.* **2018**, *11*, 2696-2767; b) Q. Wang, B.-H. Xu, Y.-X. Du, L.-Y. Kuang, Z.-S. Lin, X.-X. Gu, *Rare Met.* **2025**, *44*, 209-217.

[3] a) P. Ruan, S. Liang, B. Lu, H. J. Fan, J. Zhou, *Angew. Chem. Int. Ed.* **2022**, *61*, e202200598; b) X. Wang, Y. Pan, X. Wang, Y. Guo, C. Ni, J. Wu, C. Hao, *Ind. Crops Prod.* **2022**, *189*, 115863.

[4] T. Li, X. Li, H. Yang, Y. Zhou, X. Li, M. Su, A. Dou, P. Zhang, X. Wu, A. Naveed, J. Sumner, Y. Liu, *Mater. Today Energy* **2024**, *40*, 101513.

[5] a) A. Naveed, T. Li, A. Ali, F. Ahmad, W. A. Qureshi, M. Su, X. Li, Y. Zhou, J.-C. Wu, Y. Liu, *Small* **2024**, *n/a*, 2401589; b) R. Wang, S. Xin, D. Chao, Z. Liu, J. Wan, P. Xiong, Q. Luo, K. Hua, J. Hao, C. Zhang, *Adv. Funct. Mater.* **2022**, *32*, 2207751.

[6] T. Li, S. Hu, C. Wang, D. Wang, M. Xu, C. Chang, X. Xu, C. Han, *Angew. Chem. Int. Ed.* **2023**, *62*, e202314883.

[7] F. Tao, Y. Liu, X. Ren, J. Wang, Y. Zhou, Y. Miao, F. Ren, S. Wei, J. Ma, *J. Energy Chem.* **2022**, *66*, 397-412.

[8] a) M. R. Lukatskaya, J. I. Feldblyum, D. G. Mackanic, F. Lissel, D. L. Michels, Y. Cui, Z. Bao, *Energy Environ. Sci.* **2018**, *11*, 2876-2883; b) Y. Zhu, J. Yin, X. Zheng, A.-H. Emwas, Y. Lei, O. F. Mohammed, Y. Cui, H. N. Alshareef, *Energy Environ. Sci.* **2021**, *14*, 4463-4473.

[9] J. Cao, F. Zhao, W. Guan, X. Yang, Q. Zhao, L. Gao, X. Ren, G. Wu, A. Liu, *Small* **2024**, *n/a*, 2400221.

[10] Y. Yamada, J. Wang, S. Ko, E. Watanabe, A. Yamada, *Nat. Energy* **2019**, *4*, 269-280.

[11] a) P. Ye, X. Li, K. He, A. Dou, X. Wang, A. Naveed, Y. Zhou, M. Su, P. Zhang, Y. Liu, *J. Power Sources* **2023**, *558*, 232622; b) L. Zeng, H. He, H. Chen, D. Luo, J. He, C. Zhang, *Adv. Energy Mater.* **2022**, *12*, 2103708; c) L. Wang, W. Huang, W. Guo, Z. H. Guo, C. Chang, L. Gao, X. Pu, *Adv. Funct. Mater.* **2022**, *32*, 2108533.

[12] X. Yu, Z. Li, X. Wu, H. Zhang, Q. Zhao, H. Liang, H. Wang, D. Chao, F. Wang, Y. Qiao, H. Zhou, S.-G. Sun, *Joule* **2023**, *7*, 1145-1175.

[13] X. Zhao, Y. Wang, C. Huang, Y. Gao, M. Huang, Y. Ding, X. Wang, Z. Si, D. Zhou, F. Kang, *Angew. Chem. Int. Ed.* **2023**, *62*, e202312193.

[14] H. Zhang, Y. Zhong, J. Li, Y. Liao, J. Zeng, Y. Shen, L. Yuan, Z. Li, Y. Huang, *Adv. Energy Mater.*

2023, *13*, 2203254.

[15] T. Wei, H. Zhang, Y. Ren, L. e. Mo, Y. He, P. Tan, Y. Huang, Z. Li, D. Zhu, L. Hu, *Adv. Funct. Mater.* **2024**, *34*, 2312506.

[16] Z. Huang, Z. Li, Y. Wang, J. Cong, X. Wu, X. Song, Y. Ma, H. Xiang, Y. Huang, *ACS Energy Lett.* **2023**, *8*, 372-380.

[17] Z. Chen, R. Jiang, Y. Chen, H. Zhu, X. Tang, X. Huang, Y. Xie, J. Li, C. Zhang, L. Chen, W. Wei, L. Zhou, *Energy Storage Mater.* **2025**, *74*, 103913.

[18] Z. Hou, X. Zhang, X. Li, Y. Zhu, J. Liang, Y. Qian, *J. Mater. Chem. A* **2017**, *5*, 730-738.

[19] S. Zheng, Y. Wang, B. Luo, L. Sun, G. Duan, J. Huang, Z. Ye, *Chem. Eng. J.* **2023**, *473*, 145313.

[20] a) H. Cao, X. Huang, Y. Li, Y. Liu, Q. Zheng, Y. Huo, R. Zhao, J. Zhao, D. Lin, *Chem. Eng. J.* **2023**, *455*, 140538; b) H. Yang, Y. Cao, X. Ai, L. Xiao, *J. Power Sources* **2004**, *128*, 97-101; c) D. Feng, F. Cao, L. Hou, T. Li, Y. Jiao, P. Wu, *Small* **2021**, *17*, 2103195.

[21] N. K. Howell, G. Arteaga, S. Nakai, E. C. Y. Li-Chan, *J. Agric. Food. Chem.* **1999**, *47*, 924-933.

[22] a) S. Chen, D. Ji, Q. Chen, J. Ma, S. Hou, J. Zhang, *Nat. Commun.* **2023**, *14*, 3526; b) R. Jiang, T. Naren, Y. Chen, Z. Chen, C. Zhang, Y. Xie, L. Chen, Y. Qi, Q. Meng, W. Wei, L. Zhou, *Adv. Funct. Mater.* **2024**, *34*, 2411477.

[23] J. Yin, H. Liu, P. Li, X. Feng, M. Wang, C. Huang, M. Li, Y. Su, B. Xiao, Y. Cheng, X. Xu, *Energy Storage Mater.* **2023**, *59*, 102800.

[24] a) T. Liu, C. Lei, H. Wang, J. Li, P. Jiang, X. He, X. Liang, *Adv. Mater.* **2024**, *36*, 2405473; b) M. Shi, C. Lei, H. Wang, P. Jiang, C. Xu, W. Yang, X. He, X. Liang, *Angew. Chem. Int. Ed.* **2024**, *63*, e202407261.

[25] R. Deng, Z. He, F. Chu, J. Lei, Y. Cheng, Y. Zhou, F. Wu, *Nat. Commun.* **2023**, *14*, 4981.

[26] Q. Li, A. Chen, D. Wang, Y. Zhao, X. Wang, X. Jin, B. Xiong, C. Zhi, *Nat. Commun.* **2022**, *13*, 3699.

[27] Y. Shang, Z. Tong, D. Kundu, *ACS Energy Lett.* **2024**, *9*, 3084-3092.

[28] a) Q. Zhu, G. Sun, S. Qiao, D. Wang, Z. Cui, W. Zhang, J. Liu, *Adv. Mater.* **2024**, *36*, 2308577; b) W. Yuan, X. Nie, G. Ma, M. Liu, Y. Wang, S. Shen, N. Zhang, *Angew. Chem. Int. Ed.* **2023**, *62*, e202218386.

[29] J. Rivnay, S. C. B. Mannsfeld, C. E. Miller, A. Salleo, M. F. Toney, *Chem. Rev.* **2012**, *112*, 5488-5519.

[30] K. Gu, P. Li, G. Yi, Y. Wu, W. Yang, Z. Zhang, X. Zhang, *ChemPlusChem* **2024**, *89*, e202300475.

[31] W. Deng, T. Huang, C. Li, L. Zhang, Z. Huang, J. Sun, Z. Hu, F. Dai, *Electrochim. Acta* **2021**, *391*, 138918.

[32] J. Zheng, Q. Zhao, T. Tang, J. Yin, C. D. Quilty, G. D. Renderos, X. Liu, Y. Deng, L. Wang, D. C. Bock, C. Jaye, D. Zhang, E. S. Takeuchi, K. J. Takeuchi, A. C. Marschilok, L. A. Archer, *Science* **2019**, *366*, 645-648.



https://dspace.org/

Engineering aqueous electrolytes with vicinal sbased organic additives for highly reversible zincion batteries

Li, Teng; Naveed, Ahmad; Zheng, Jiongzhi; Chen, Bixian; Jiang, Mingfeng ...

2025-05-19
Wiley
https://doi.org/10.1002/ange.202424095
Li T, Naveed A, Zheng J, et al., (2025) Engineering aqueous electrolytes with vicinal sbased organic additives for highly reversible zincion batteries. Angewandte Chemie, Volume 137, Issue 21, May 2025. Article number e202424095

Downloaded from a DSpace repository. https://dspace.org/